Sulfur dioxide (SO$_2$) from MIPAS in the upper troposphere and lower stratosphere 2002–2012

M. Höpfner[1], C. D. Boone[2], B. Funke[3], N. Glatthor[1], U. Grabowski[1], A. Günther[1], S. Kellmann[1], M. Kiefer[1], A. Linden[1], S. Lossow[1], H. C. Pumphrey[4], W. G. Read[5], A. Roiger[6], G. Stiller[1], H. Schlager[6], T. von Clarmann[1], and K. Wissmüller[6]

[1]Institute for Meteorology and Climate Research, Karlsruhe Institute of Technology, Karlsruhe, Germany
[2]Department of Chemistry, University of Waterloo, Waterloo, Ontario, Canada
[3]Instituto de Astrofísica de Andalucía, CSIC, Granada, Spain
[4]School of GeoSciences, The University of Edinburgh, Edinburgh EH9 3JN, UK
[5]Jet Propulsion Laboratory, California Institute of Technology, Pasadena, CA 91109-8099, USA
[6]Institut für Physik der Atmosphäre, Deutsches Zentrum für Luft und Raumfahrt, Oberpfaffenhofen, Germany

Correspondence to: M. Höpfner (michael.hoepfner@kit.edu)

Abstract. Vertically resolved distributions of sulfur dioxide (SO$_2$) with global coverage in the height region from the upper troposphere to ~ 20 km altitude have been derived from observations by the Michelson Interferometer for Passive Atmospheric Sounding (MIPAS) on Envisat for the period July 2002 to April 2012. Retrieved volume mixing ratio profiles representing single measurements are characterized by typical errors in the range of 70–100 pptv and by a vertical resolution ranging from 3 to 5 km. Comparison with observations by the Atmospheric Chemistry Experiment Fourier transform spectrometer (ACE-FTS) revealed a slightly varying bias with altitude of −20 to 50 pptv for the MIPAS data set in case of volcanically enhanced concentrations. For background concentrations the comparison showed a systematic difference between the two major MIPAS observation periods. After debiasing, the difference could be reduced to biases within −10 to 20 pptv in the altitude range of 10–20 km with respect to ACE-FTS. Further comparisons of the debiased MIPAS data set with in situ measurements from various aircraft campaigns showed no obvious inconsistencies within a range of around ±50 pptv. The SO$_2$ emissions of more than 30 volcanic eruptions could be identified in the upper troposphere and lower stratosphere (UTLS). Emitted SO$_2$ masses and lifetimes within different altitude ranges in the UTLS have been derived for a large part of these eruptions. Masses are in most cases within estimations derived from other instruments. From three of the major eruptions within the MIPAS measurement period – Kasatochi in August 2008, Sarychev in June 2009 and Nabro in June 2011 – derived lifetimes of SO$_2$ for the altitude ranges 10–14, 14–18 and 18–22 km are 13.3 ± 2.1, 23.6 ± 1.2 and 32.3 ± 5.5 days respectively. By omitting periods with obvious volcanic influence we have derived background mixing ratio distributions of SO$_2$. At 10 km altitude these indicate an annual cycle at northern mid- and high latitudes with maximum values in summer and an amplitude of about 30 pptv. At higher altitudes of about 16–18 km, enhanced mixing ratios of SO$_2$ can be found in the regions of the Asian and the North American monsoons in summer – a possible connection to an aerosol layer discovered by Vernier et al. (2011b) in that region.

1 Introduction

The background aerosol loading of the stratosphere has been found to increase since about the year 2000 (Hofmann et al., 2009; Vernier et al., 2011b). Due to the negative radiative forcing of stratospheric sulfate aerosol, this trend has been discussed as part of the explanation for a slowdown in the rise of global temperatures (the so-called global warming hiatus) since the turn of the millennium (Solomon et al., 2011; Fyfe et al., 2013a, b; Haywood et al., 2013; Santer et al.,

2014). Hofmann et al. (2009) explained the rising strato-spheric aerosol levels with an increase in the anthropogenic sulfur dioxide (SO$_2$) production in South East Asia while Vernier et al. (2011b) opposed this view by showing the increasing influence from sulfate injection of moderate tropical volcanic eruptions into the stratosphere. Recently, Ridley et al. (2014) have used ground-based and balloon-borne observations to demonstrate that especially at mid- and high latitudes the aerosol loading within the altitude range between the tropopause and 15 km contribute strongly to the volcanic aerosol forcing during the last decade.

As a basis for studying these processes with the aid of atmospheric models, it is essential to get global information about the amount of SO$_2$ reaching stratospheric altitudes. Measurements of SO$_2$ in the upper troposphere and lower stratosphere (UTLS) are, however, sparse. In situ observations from aircraft campaigns are highly accurate (see also Sect. 2.6). However, they provide mainly snapshots of the atmospheric state, which might be influenced by the sampling tailored specifically to the campaign objective. Global observations from satellite nadir sounding instruments provide horizontally highly resolved pictures of SO$_2$ distributions emitted by strong sources, like volcanoes (Theys et al., 2013, and references therein). While most analysis methods of nadir sounding observations provide vertical column amounts of SO$_2$, various recent studies indicate that volcanic plume heights can be derived (Yang et al., 2010; Van Gent et al., 2012; Rix et al., 2012; Carboni et al., 2012; Clarisse et al., 2014; Fromm et al., 2014).

Owing to their observation geometry, limb-sounding measurements are especially suited to obtain profile information of atmospheric constituents. In the microwave spectral region, Read et al. (1993) retrieved SO$_2$ concentrations from the Microwave Limb Sounder (MLS) on the Upper Atmosphere Research Satellite (UARS) in the aftermath of the eruption of Mt. Pinatubo and Pumphrey et al. (2015) analysed SO$_2$ signatures from various volcanic eruptions measured by the MLS instrument on the Aura satellite. In the mid-infrared, Doeringer et al. (2012) used solar occultation spectra measured by the Atmospheric Chemistry Experiment Fourier transform spectrometer (ACE-FTS) to reconstruct vertical profiles of SO$_2$ following the eruption of the Sarychev volcano in June 2009.

In the following we present global altitude-resolved distributions of SO$_2$ between about 10 and 20 km as retrieved from infrared limb-emission observations by MIPAS (Michelson Interferometer for Passive Atmospheric Sounding) between June 2002 and April 2012. This data set is derived from single MIPAS limb spectra and complementary to the one presented in Höpfner et al. (2013) which was reconstructed from monthly and 10° zonally averaged spectra, covering the height region between 15–20 and 40 km altitude. Thus, the present data set allows us to exploit the full spatial and temporal coverage and resolution of the MIPAS observations.

In Sect. 2 we describe the measurements and the retrieval scheme and characterize the data set comprising vertical resolution and error estimation. This is followed by a comparison with independent remote sensing and in situ observations of SO$_2$ in the UTLS region. Besides an overview over the whole data set, the main subject of Sect. 3 is the analysis of volcanic plumes with respect to the derivation of eruption masses and lifetimes of SO$_2$ from major volcanic events. The global non-volcanic background distribution of SO$_2$ is presented at the end of Sect. 3 and final conclusions are drawn in Sect. 4.

2 The MIPAS SO$_2$ data set

2.1 Instrument

MIPAS (Fischer et al., 2008) was operated on the sun-synchronous polar orbiting satellite Envisat. Envisat was launched on 1 March 2002 and lost ground contact on 8 April 2012. The MIPAS instrument is a limb sounder measuring the thermal radiation emitted by the atmosphere in the region 685–2410 cm^{-1} by means of a Fourier transform spectrometer (ESA, 2000).

Two main periods of MIPAS operation can be distinguished: period 1 (P1) lasted from June 2002 until April 2004 and period 2 (P2) from January 2005 until April 2012. During P1 the spectral resolution was 0.025 cm^{-1} (unapodized). The latitudinal distance between subsequent limb scans was 530 km, where each limb scan consisted of 17 tangent views with 3 km sampling steps in the UTLS region. During P2 the spectral resolution was set to 0.0625 cm^{-1} (unapodized), thereby reducing the measurement time per spectrum. This led to finer horizontal (420 km) and vertical (1.5 km in the UTLS region) sampling patterns.

For the retrieval of SO$_2$ described in this paper, level-1b calibrated spectra version 5 as provided by ESA have been used (Nett et al., 2002).

2.2 Retrieval

In contrast to the MIPAS data set of SO$_2$ published by Höpfner et al. (2013), which was reconstructed from monthly and zonal averaged spectra, the present retrieval has been performed on the basis of single limb scans. The standard MIPAS IMK-IAA data processing scheme has been applied as described in detail by von Clarmann et al. (2003) and von Clarmann et al. (2009). The retrieval method is a constrained non-linear least squares multi-target fitting procedure of measured limb radiances. Spectral fitting intervals which have been applied for the reconstruction of SO$_2$ are listed in Table 1. In addition to the spectral region of the ν_3 band around 1370 cm^{-1} (Höpfner et al., 2013) we have used lines from the weaker ν_1 band around 1130 cm^{-1} to minimize errors due to saturation in case of enhanced concentrations. Beside the volume mixing ratios of SO$_2$, jointly re-

Table 1. Spectral windows for MIPAS SO₂ retrieval [cm⁻¹].

MIPAS period	
P1 (2002–2004)	P2 (2005–2012)
1128.2000–1129.4250	1128.1875–1129.4375
1132.1250–1132.7500	1132.1250–1132.7500
1136.3250–1136.8750	1136.3125–1136.8750
1139.4500–1141.0000	1139.4375–1141.0000
1142.0000–1143.3000	1142.0000–1143.3125
1366.5750–1368.2500	1366.5625–1368.2500
1369.9500–1370.6250	1369.9375–1370.6250
1371.1250–1371.9250	1371.1250–1371.9375
1376.0000–1376.6250	1376.0000–1376.6250

Table 2. Results of retrieval simulations for enhanced profiles. The vmr values of SO₂ at the profile maximum and the integrated column amounts between 10 and 25 km are reported (Ref. is reference, Res. is result, Diff. is difference = (Res.−Ref.)/Ref. × 100).

VMR max			Column (10–25 km)		
Ref. [ppbv]	Res. [ppbv]	Diff. [%]	Ref. [DU]	Res. [DU]	Diff. [%]
1.08	1.01	−6.34	0.12	0.12	1.23
5.08	4.43	−12.78	0.52	0.52	−0.13
10.08	8.19	−18.71	1.02	1.00	−1.72
50.08	31.02	−38.06	5.03	4.67	−7.01
100.08	49.90	−50.14	10.03	8.57	−13.97
500.08	114.14	−77.18	50.10	22.33	−54.83

trieved parameters are altitude profiles of the main spectrally interfering species H₂O, O₃, N₂O and CH₄. Height distributions of further trace gases exhibiting minor signatures in the spectral region of interest are taken either from previous steps in the retrieval chain (HNO₃, N₂O₅, CFC−12, HCN, PAN, C₂H₂) or are based on climatological profiles (HCFC−22, CFC−113, CFC−114, HCFC−142b). The atmospheric temperature profile, the instrumental line of sight and spectral calibration correction are likewise imported from previous retrieval steps.

Regularization of the retrieval is necessary since the altitude grid distance of the atmospheric profiles is 1 km and, thus, smaller than the vertical tangent point spacing of 1.5–3 km. Here we have applied a standard first-order Tikhonov regularization scheme (Tikhonov, 1963; Steck, 2002). This scheme constrains the reconstructed profiles by minimizing along with the spectral residual also the first derivative of the vertical profile. Thus, the regularization introduces a smoothness of the result but avoids any biasing with respect to some absolute volume mixing ratio (vmr). The resulting vertical resolution varies from 3 to 5 km in the altitude range between 10 and 20 km.

The IMK-IAA MIPAS data which are used in this work are versions V5H_SO2_20, V5R_SO2_220 and V5R_SO2_221.

2.3 Error estimation

An estimate of altitude-dependent retrieval errors of various sources has been performed separately for different locations belonging to both measurement periods and for volcanically perturbed and unperturbed atmospheric situations. Figure 1 shows the resulting mean error profiles for each of the four categories. Estimated errors are split into one purely random term, due to measurement noise, and "systematic" terms, due to instrumental, spectroscopic and errors in predetermined parameters, like temperature and line-of-sight pointing. Note, however, that the "systematic" error contains also random contributions with different time-scales, e.g. radiometric calibration. The random error due to measurement
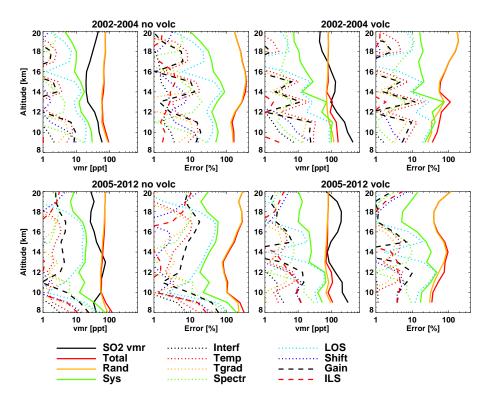
noise leads to vmr errors which are at first-order independent of the SO₂ amount in the atmosphere. With around 70–100 pptv it is the dominant error contribution when single (non-averaged) profiles are considered. In the case of averaging, systematic errors become more important. These are estimated to about 10–75 pptv (10–180 %) for cases without volcanic influence and 10–110 pptv (10–75 %) in volcanically enhanced conditions (Fig. 1).

In contrast to other trace gases measured with MIPAS, the dynamic range of SO₂ vmr values in the atmosphere can vary significantly because of volcanic activity. This can introduce errors in the retrieved profiles due to saturation effects in the radiative transfer. We have estimated these uncertainties by sensitivity studies. Table 2 shows the results depending on the value of the maximum of the assumed SO₂ vmr profile. The retrieved vmr values show maximum concentrations underestimated by −13 % for 5 ppbv and −50 % for a reference of 100 ppbv. Partial column amounts over a certain altitude range around the maximum of the vmr profile are much less affected. The underestimation here reaches from −0.1 % for the profile with a maximum of 5 ppbv to −14 % for 100 ppbv at the maximum. This result indicates that the error of the maximum vmr value is mainly caused by the regularization smoothing constraint while saturation effects appear for profiles with vmr values above 50–100 ppbv.

2.4 Validation

2.4.1 Comparison with ACE-FTS

We have performed a comparison of MIPAS altitude profiles of SO₂ with those of the ACE-FTS instrument (research product version 3.0). ACE-FTS is one of the instruments belonging to the Atmospheric Chemistry Experiment space mission launched in August 2003 (Bernath et al., 2005). The Fourier transform spectrometer measures infrared solar occultation spectra from 750 to 4400 cm⁻¹ with a spectral resolution of 0.02 cm⁻¹ at sunrise and sunset during each orbit. The vertical resolution of the retrieved profiles of atmo-
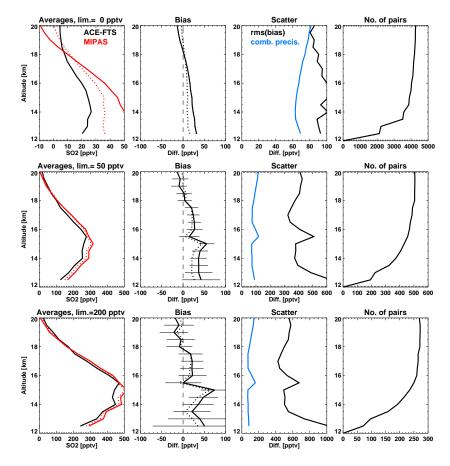
Figure 1. Four pairs of plots showing single profiles error estimates for MIPAS SO₂. Within each pair the left plot represents the absolute and the right plot the relative errors. Left pairs: no clear volcanic enhancement; right pairs: volcanically enhanced profiles; top: MIPAS period P1; bottom: MIPAS period P2. Meaning of abbreviations in the legend: "Total" is the combined random and systematic error; "Rand" is the random error; "Sys" is the systematic error; "Interf" is the error due to uncertainty of interfering species; "Temp" is the temperature error; "Tgrad" is the error due to neglect of a horizontal temperature gradient; "Spectr" is the spectroscopic data error; "LOS" is the error due to line-of-sight pointing uncertainty; "Shift" is the spectral shift error, "Gain" is the radiometric gain calibration uncertainty; "ILS" is the uncertainty of instrumental line shape.

spheric traces gases is about 3–4 km as set by the instrument's field of view. More specific information on the reconstruction of SO₂ vertical distributions from ACE-FTS measurements can be found in Doeringer et al. (2012).

In Fig. 2 the comparison of SO₂ profiles between MIPAS and ACE-FTS is shown for collocated observations using a match criterion of 500 km and 5 h. Furthermore, the profiles have been grouped into one part to represent background conditions with mixing ratios smaller than 50 pptv (top row in Fig. 2) and two groups to represent enhanced mixing ratios with at least one vmr value up to 20 km larger than 50 and 200 pptv (middle and bottom row of Fig. 2 respectively). In the case of the background conditions, there is a clear bias with larger MIPAS mixing ratios of up to 30 pptv below 18 km and up to 15 pptv lower MIPAS values for altitudes between 18 and 20 km. The combined precision estimates of both instruments (blue curves in the third column) are slightly smaller than the standard deviation (SD) of the differences. As will be shown below, this is caused by the residual atmospheric variability within the limits of the collocation criterion. In the case of enhanced SO₂ vmr values, differences between MIPAS and ACE-FTS are generally in

the range of ±30 pptv, reaching values of ±50–100 pptv only at a few altitudes. However, as shown by the error bars in the second row of Fig. 2, these differences lie mostly inside the SD of the differences and, thus, are not significant. The large difference between the black and blue curves in the middle and bottom plot of the third column (Fig. 2) is very probably due to the strong atmospheric variability of SO₂ under volcanic influence.

Figure 3 presents a closer look at the comparison of collocated measurements for the background case. Here we have distinguished matches during MIPAS periods P1 (top) and P2 (bottom). Additionally, during P2 only profiles during periods of low volcanic activity have been selected which was not necessary for P1 since there was no significant volcanic influence when both instruments measured simultaneously. This representation reveals that the typical bias of up to 30 pptv for the SO₂ background only appears during period P2 while during P1 no significant bias between the two instruments can be detected. We suppose that this fact is due to the higher spectral resolution during P1 which makes the retrieval of small spectral signatures more robust. Furthermore, there is a very good agreement between the combined estimated in-
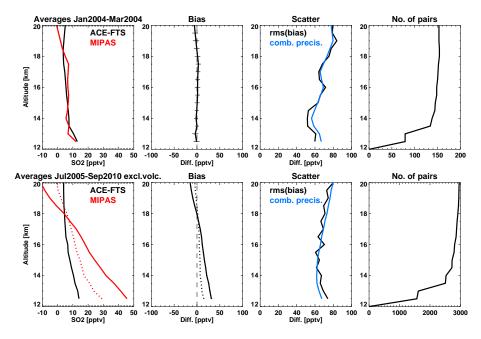
Figure 2. Comparison of MIPAS and ACE-FTS collocated single profile measurements. Left column: average profiles (red solid: MIPAS original data set, red dotted: MIPAS data set after debiasing; cf. Sect. 2.5). Second column: mean differences MIPAS-ACE-FTS (solid: before, dotted: after debiasing) together with their standard error (error bars; not visible in the top row since these are smaller than the line thickness) calculated as their SD (see third column) divided by the square root of the number of pairs (see last column). Third column: SD of the single differences (black line) and the mean value of the combined estimated precision of the two instruments (blue line). Fourth column: number of collocated pairs used for comparison at each altitude. Top row: only those pairs are selected where ACE-FTS profile values are smaller than 50 pptv up to 20 km altitude. Middle row: only those pairs are selected where ACE-FTS profile values are above 50 pptv at least at one altitude level up to 20 km. Bottom row: same as middle row but for a lower limit of 200 pptv.

strument precision and the SD of the profile differences (third column in Fig. 3). This is due to the selection of periods with very low volcanic activity which, in addition to the criterion on small vmr values of SO$_2$, leads to a reduction of atmospheric variability in the data set. This demonstrates that the combined precision estimates of MIPAS and ACE-FTS are realistic.

2.4.2 Comparison with retrievals from mean MIPAS spectra and the monthly averaged ACE-FTS data set

Here we analyse the agreement between the MIPAS SO$_2$ data retrieved from monthly zonal mean spectra (Höpfner et al., 2013) (called MIPASmon in the following) and the present single scan data set. Figure 4 shows the comparison of average monthly mean profiles between the two MI-

PAS data sets and ACE-FTS for background (top) and volcanically perturbed cases (bottom). For the background situation, MIPAS monthly mean profiles from single scan retrievals show similar differences either to MIPASmon or the ACE-FTS data set. This is in agreement with the comparisons of collocated profiles between MIPAS and ACE-FTS described in the previous section. The background profiles of MIPASmon and ACE-FTS compare very well. In contrast, the comparison of volcanically enhanced monthly mean profiles (Fig. 4, bottom) reveals a good agreement between ACE-FTS and MIPAS single scan retrievals while MIPASmon seems to underestimate the atmospheric SO$_2$ content by up to 100 pptv. Such an underestimation of SO$_2$ in MIPASmon for volcanically enhanced periods has already been suspected when comparing the SO$_2$ distribution of July 2009 between ACE-FTS and MIPASmon retrievals (Höpfner et al., 2013).

Figure 3. Same as top row in Fig. 2 but (1) separated in MIPAS phase 1 (top row) and phase 2 (bottom row) observation periods and (2) excluding periods with strong volcanic influence (January–June 2005, May–November 2006, October 2007, July–December 2008, June–December 2009).

When comparing MIPAS and MIPASmon profiles of SO₂ separately for MIPAS periods P1 and P2 and additionally excluding volcanically enhanced periods (see Fig. 5), we reach the same conclusion as from the comparison with ACE-FTS in Fig. 3: in P1 the background distribution compares well between both data sets while during P2 a typical bias of the MIPAS single scan retrieved data of up to 30 pptv is apparent.

2.5 Debiasing

The presented comparisons have revealed a distinct height-dependent bias between the SO₂ retrievals from MIPAS periods P1 and P2 of up to about 30 pptv down to about 12 km. Most observations further indicate that this bias affects the observations during measurement period P2. Thus, for the subsequent discussion of the whole data set from 2002 to 2012 we have applied an altitude- and latitude-dependent bias-correction to the data from period P2. This 2-dimensional correction pattern has been determined as the difference between the mean SO₂ distributions (height vs. latitude) of period P1 and period P2 where, for both periods, months of major volcanic influence have been excluded. The spatial correction pattern as shown in Fig. 6 does not vary strongly with latitude down to about 10 km altitude. It is generally positive above 17–18 km and negative below, reaching values of −150 pptv at the lowest altitudes between 6 and 10 km.

The comparisons with ACE-FTS and MIPAS monthly mean retrievals as discussed above and as shown in Figs. 2–5 have been repeated for the debiased data set (bold dotted

lines in these figures). The results now show a much better consistency between the two measurement periods with remaining maximum differences of about 10–15 pptv at 13–14 km and of a few tens of pptv at lowest altitudes. In the following we will restrict the discussion to altitudes above 10 km where remaining differences between the data sets of P1 and P2 are around 10 pptv.

2.6 Comparison of the debiased data set with in situ observations

The comparison of MIPAS SO₂ with ACE-FTS and MIPASmon is only possible for altitudes above 12.5 and 15 km respectively. The altitude region between about 8 and 12 km has been covered mainly by in situ observations from aircraft.

In Fig. 7 we show a collection of published airborne measurements of SO₂ mainly observed before the year 2000 (Jaeschke et al., 1976; Inn and Vedder, 1981; Meixner, 1984; Möhler and Arnold, 1992; Reiner et al., 1998; Thornton et al., 1999; Jaeschke et al., 1999; Curtius et al., 2001). These are compared to MIPAS data of similar geographic range and season excluding periods of strong volcanic influence. Furthermore, the MIPAS data are subdivided into measurement periods P1 (green) and P2 (blue, solid) because of the debiasing of measurement period P2 with respect to P1 as described above. In general the MIPAS data are in the range of in situ observations. In the northern high and mid-latitudes, e.g. in Meixner (1984), Möhler and Arnold (1992) and Reiner et al. (1998), the values increase with lower altitudes, which is re-
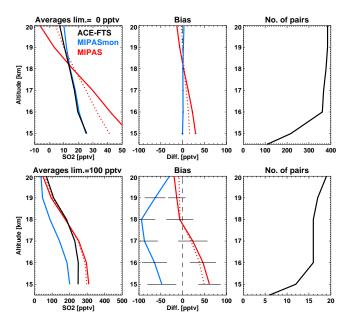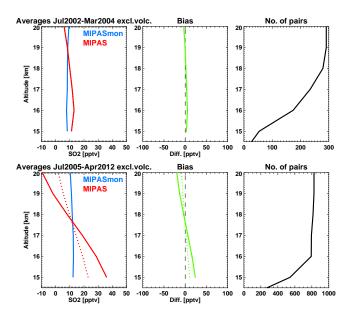
Figure 4. Comparison between monthly mean profiles from ACE-FTS, MIPASmon (Höpfner et al., 2013) and MIPAS. Left: average profiles (red solid: MIPAS original data set, red dotted: MIPAS data set after debiasing). Middle: mean differences (blue: MIPASmon – ACE-FTS, red: MIPAS – ACE-FTS, red solid: before debiasing, red dotted: after debiasing) together with their standard error (error bars; not visible in the top row since these are smaller than the line thickness). Right: number of collocated pairs of monthly mean values used for comparison at each altitude. Top: only those pairs are selected where MIPASmon profile values are smaller than 50 pptv up to 20 km altitude. Bottom: only those pairs are selected where MIPASmon profile values are above 100 pptv at least at one altitude level up to 20 km.

Figure 5. Same as top row in Fig. 4 but (1) only for MIPAS-mon and MIPAS, (2) separated in MIPAS phase 1 (top row) and phase 2 (bottom row) observation periods and (3) excluding periods with strong volcanic influence (October–December 2002, July 2003, January–June 2005, May–November 2006, October 2007, July–December 2008, June–December 2009, November–December 2010, July–September 2011).

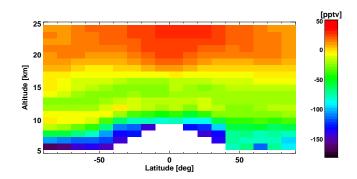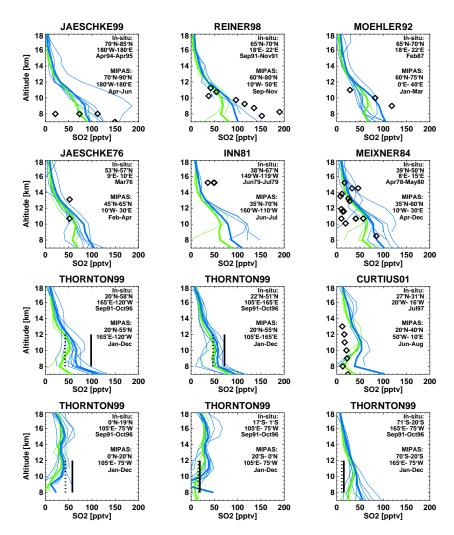**Figure 6.** Bias correction applied to the MIPAS data set from period P2 (2005–2012).

flected in the MIPAS data set. At more remote regions like over the equatorial and southern Pacific Ocean, Thornton et al. (1999) observed in general lower SO₂ mixing ratios than in the Northern Hemisphere (bottom row in Fig. 7). This is reflected mainly by the MIPAS data which show a weaker vertical gradient compared to the observations in the north and are in magnitude similar to the Thornton et al. (1999) observations in the equatorial region. However, at southern subtropical and mid-latitudes MIPAS values are higher than the in situ data by 20–30 pptv.

A comparison with a more recent set of in situ observations is presented in Fig. 8. The data have been collected by DLR-IPA (Deutsches Zentrum für Luft- und Raumfahrt – Institute für Physik der Atmosphäre) and MPI-K (Max-Planck-Institut für Kernphysik) using a jointly developed ion trap chemical ionization mass spectrometer (ITCIMS), described in Speidel et al. (2007), during several measurement campaigns (Schlager et al., 2006; Fiedler et al., 2009b, 2011; Waddicor et al., 2012; Barth et al., 2014; Roiger et al., 2014).

In contrast to the behaviour of SO₂ with altitude shown before, this time the vmr values in the northern mid- to high

latitudes (first two rows in Fig. 8) do not show a distinct increase towards lower altitudes, which is different from MIPAS. Also, the absolute in situ measured vmr values are in most cases smaller than MIPAS, especially at altitudes below 10 km. In contrast, the equatorial and southern hemispheric ITCIMS data from AMMA, SCOUT-O3 and TROCCINOX are higher compared to MIPAS. The in situ data from the ESMVal-Antarktis campaign are, with around 10 pptv, comparable to the South Pacific data of Thornton et al. (1999) and lower than MIPAS up to 13 km by up to 40 pptv. Above 13 km differences are reduced to about 10 pptv.
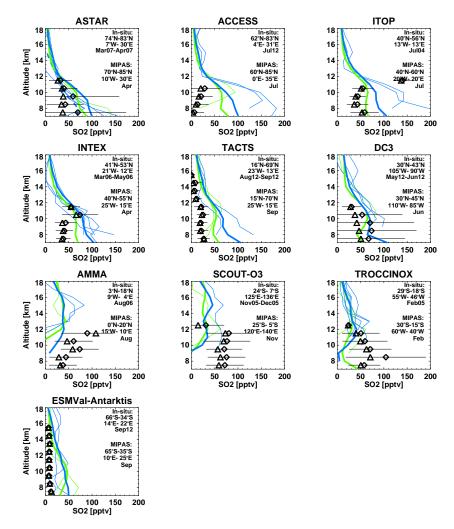
Obviously, it is difficult to gain a coherent picture of the uncertainty of the MIPAS background SO₂ data set in the

Figure 7. Comparison between in situ and debiased MIPAS observations of SO₂. Green lines indicate MIPAS measurements before April 2004 and blue lines after January 2005 (solid thin lines: mean of each year, solid bold lines: mean of all profiles). Black diamonds show the in situ observations based on publications as given in the plot title (JAESCHKE76: Jaeschke et al. (1976), INN81: Inn and Vedder (1981), MEIXNER84: Meixner (1984), MOEHLER92: Möhler and Arnold (1992), THORNTON99: Thornton et al. (1999), CURTIUS01: Curtius et al. (2001), JAESCHKE99: Jaeschke et al. (1999), REINER98: Reiner et al. (1998). In the case of THORNTON99, the data from Thornton et al. (1999, Plate 3) have been subdivided into five regions over the Pacific (bold black lines: mean, dotted: median). Periods with strong volcanic influence have been excluded from the MIPAS data (see caption of Fig. 5).

lowermost stratosphere/upper troposphere from comparison with in situ measurements. First, the variability of SO₂ in the UTLS is quite large. We have tried to restrict the MIPAS data to background situations while the in situ data might contain cases in which volcanic plumes are sampled. Unfortunately, the real matches between in situ and MIPAS data are too sparse to get robust statistics – so we had to compare with seasonal mean MIPAS data. Second, aircraft campaigns are snapshots and even are often dedicated to specific objectives which might not be representative of the atmospheric situation in general. Third, even the atmospheric background situation might be different due to changes in industrial emission patterns influencing the UTLS distributions of SO₂.

In summary, for the region between 7 and 15 km the MI-PAS data set of SO₂ (especially above 10 km) seems to be in accordance with the set of in situ observations within its estimated systematic error of a few tens of ppt. Thus, in the following we will restrict the discussion to the debiased data set and to altitudes above 10 km, where remaining differences between the debiased data of P1 and P2 are around 10–20 pptv.

Figure 8. Comparison between in situ airborne ITCIMS observations and the debiased MIPAS data set of SO$_2$. Green lines indicate MIPAS measurements before April 2004 and blue lines after January 2005 (solid thin lines: monthly mean for each year, solid bold lines: mean of all profiles, dashed bold lines: monthly mean for year of in situ observation). Black diamonds and horizontal bars show the mean values of the in situ observations as well as their 1σ variability. The median value of the in situ measurements is indicated by black triangles. Periods with strong volcanic influence have been excluded from the MIPAS data (see caption of Fig. 5).

3 Results and discussion

3.1 SO$_2$ distributions

As an example for daily distributions from MIPAS, Fig. 9 shows volume mixing ratios of SO$_2$ at the altitude levels 18, 20 and 22 km for 3 days after the eruption of the Nabro volcano on 12 June 2011. The plume of enhanced concentrations is clearly visible on 17 June reaching from northern Africa over the mid-east to South East Asia at 18 and 20 km, while no clear enhancements are visible at 22 km altitude. This global dispersion is similar to observations by IASI (Clarisse et al., 2014; Fromm et al., 2014). One week later, on 24 June, the plume filled a large area of the Asian monsoon region. Its extension towards the west reached 0° longitude over northern Africa. Even at 22 km, enhanced values

of SO$_2$ could be observed within a restricted area reaching from the Arabian Peninsula over India and southern China. One month later, on 22 July, the plume at 18 km extended around the globe from the tropics to high northern latitudes, while at 20 km it remained within the tropics/subtropics and at 22 km no clear enhancements could be observed anymore. In the MIPAS data set enhanced values of lower stratospheric SO$_2$ over the Northern Hemisphere can be observed even until mid-/end of September 2011. Of course it must be kept in mind that due to the limited vertical resolution, high volume mixing ratios in the retrieved profiles detected up to 22 km altitude do not guarantee that volcanic SO$_2$ actually reached these heights. Taking into account, however, the half-width of the averaging kernel (3–5 km), it is very probable that the plume extended at least to heights of 20 km.
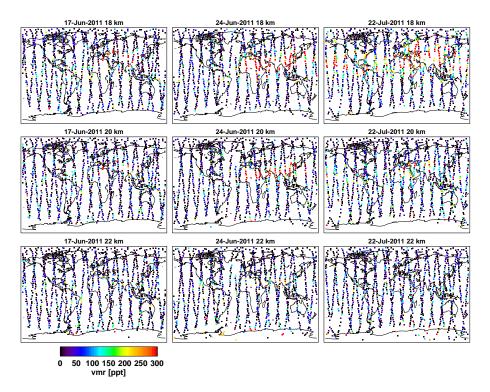
Figure 9. Example from the MIPAS data set of SO₂ for 3 days and at three altitude levels after the eruption of Nabro on 12 June 2011. Note that the colour scale does not cover the entire range of the data such that vmr values > 300 pptv are set to the colour at 300 pptv (red) and negative values to 0 (black).

To give an overview over the whole measurement period, Figs. 10–12 show the data set grouped as bins of 2-day and 10° zonal means. The most obvious signals influencing the time series are due to volcanic eruptions which have been indicated by triangles and abbreviations (see Table 3). A quantitative analysis of the emitted masses of SO₂ from these volcanic events is discussed in Sect. 3.2. In the subsequent Sect. 3.3 we try to extract the global distribution and the temporal behaviour of the non-volcanic background of SO₂ in the UTLS.
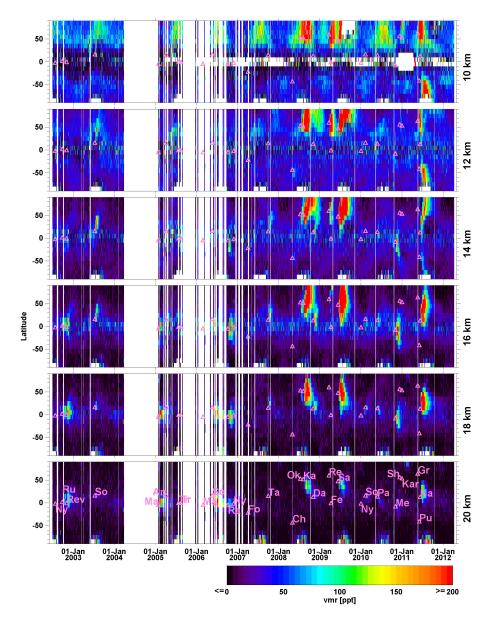
3.2   Volcanic SO₂ mass and lifetime

As noticed above, the strongest contribution to the variability of SO₂ volume mixing ratios in our data set is caused by volcanoes. Though not as strong as the one of Pinatubo in 1992, many mid-scale volcanic eruptions occurred in the period 2002–2012. Partly overlapping the measurement period of MIPAS there exist observations of volcanic SO₂ by the microwave limb-emission sounder MLS on Aura (Pumphrey et al., 2015). Though not being as sensitive to SO₂ as the mid-infrared observations, measurements in the microwave have the advantage of being less affected by particles like aerosols or thin clouds in the line of sight.

In Fig. 13 we show an example of the development of the total mass of SO₂ as calculated from MLS and MIPAS volume mixing ratios during a period of time around the erup-

tion of Sarychev on 12 June 2009. Directly after the eruption, total SO₂ masses of both instruments increase. However, MLS shows a faster rise and larger maximum values. After a few weeks, the global SO₂ masses of the instruments start to agree, showing a similar decline afterwards.

We interpret this behaviour as an underestimation of the MIPAS SO₂ masses directly after strong volcanic eruptions. This is supported by the assumption that the major mass of SO₂ is injected into the UTLS region during the eruption and decreasing afterwards, as observed e.g. by various nadir sounding satellite instruments. First, one reason for this underestimation is the influence of volcanic particles on the MIPAS measurements: spectra strongly affected by aerosols or clouds are excluded from the retrieval. As described in Höpfner et al. (2013) the cloud clearing algorithm excludes tangent views with a particle volume density of about 1–2 $\mu m^3 cm^{-3}$ along the line of sight. This causes a sampling artifact where non-plume air masses are favoured. Second, the presence of largely enhanced concentrations of SO₂ leads to saturation of the spectral lines and, thus, to an underestimation in the retrieval as described in Sect. 2.3. Maximum volume mixing ratios derived from MIPAS after strong volcanic eruptions are around 13 ppbv of SO₂. These are concentrations where saturation effects, especially when considering partial column amounts, are in the range of a few percent (cf. Table 2). Thus, we do not consider saturation to be

Figure 10. Global time series of colour-coded SO$_2$ distributions at various altitudes with a time resolution of 2 days. The colour scale is restricted to 0–200 pptv: negative and values larger than 200 pptv are given the colour belonging to 0 and 200 pptv respectively. Volcanic eruptions are indicated at the latitude of their location (for details see Table 3).

as important as the cloud clearing for the underestimation of SO$_2$ masses. Third, the sampling of the horizontally restricted plume directly after the eruption by limb-sounding instruments results in errors in total mass estimation which might be slightly worse in case of MIPAS due to a less dense along-track sampling compared to MLS.

In order to compile a climatology of SO$_2$ masses emitted by volcanoes, we have fitted the MIPAS observations to a parametric model with exponential decay, similar to Pumphrey et al. (2015):

$$M_{\Delta h_i}(t) = M_{\Delta h_i}(t_0) \times \exp\left(-\frac{t - t_0}{\tau_{\Delta h_i}}\right). \qquad (1)$$

$M_{\Delta h_i}(t)$ are the background-subtracted zonal mean masses of SO$_2$ observed by MIPAS binned over 5 days within the latitude range where elevated signals are observed and within the altitude range Δh_i. The background values have been determined using the observations just before the eruption time t_0. The fitting parameter $M_{\Delta h_i}(t_0)$ denotes the emitted mass at time t_0 and $\tau_{\Delta h_i}$, the e-folding lifetime of SO$_2$, at Δh_i.

For the calculation of masses, the MIPAS retrievals of SO$_2$ volume mixing ratios have been combined with the pressure–temperature data set also derived from MIPAS (von Clarmann et al., 2003) to obtain vertical profiles of number densities. These profiles have been integrated in the verti-
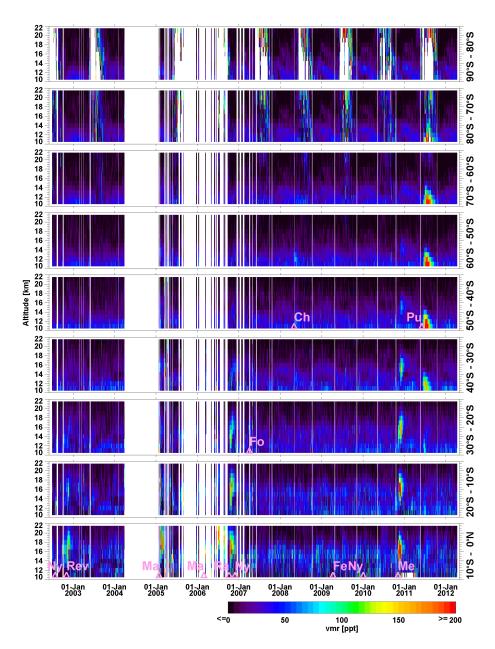
Figure 11. Time series of colour-coded SO₂ volume mixing ratio profiles for 10° latitude bins in the Southern Hemisphere with a time resolution of 2 days. The colour scale is restricted to 0–200 pptv: negative and values larger than 200 pptv are given the colour belonging to 0 and 200 pptv respectively. Volcanic eruptions are indicated at the latitude bin of their location (for details see Table 3).

cal over the respective layer thickness to obtain partial column amounts. Subsequently, these data have been averaged within 10° latitude bins and multiplied by the zonal area to obtain zonal masses of SO₂. Subsequently, for the calculation of $M_{\Delta h_i}(t)$ the masses of those zonal bands, which relative to their background values were clearly affected by the respective eruption, have been summed up.

Unlike Pumphrey et al. (2015) we have chosen to perform an altitude-dependent fit within three atmospheric layers ($\Delta h_1 = 10$–14 km, $\Delta h_2 = 14$–18 km, $\Delta h_3 = 18$–22 km).

Furthermore, due to the underestimated SO₂ masses directly after a volcanic eruption, as discussed above, the fitting period initiates not at t_0 but when linear behaviour of $\ln(M_{\Delta h_i}(t))$ starts and ends when no enhanced signal compared to the background is detected.

In the fifth row of Table 3 the resulting values of $M_{\Delta h_i}(t_0)$ and $\tau_{\Delta h_i}$ for all volcanic eruptions which could be detected within the MIPAS data set are presented for each of the three atmospheric layers. The total masses are indicated in bold face. An independent fit of $M_{\Delta h_i}(t_0)$ and $\tau_{\Delta h_i}$ has
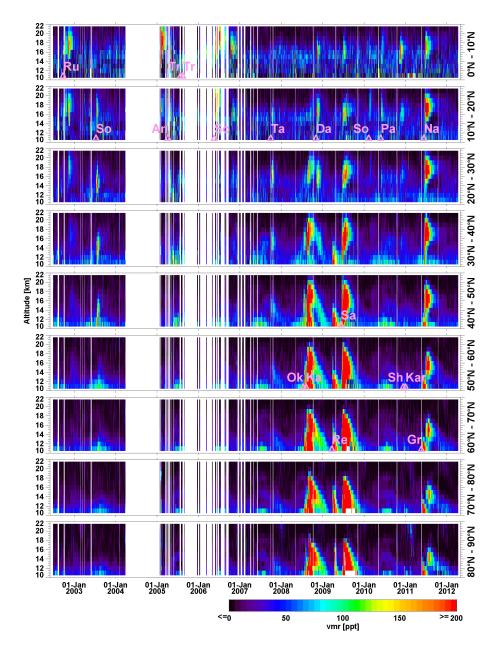
Figure 12. Same as Fig. 11 but for the Northern Hemisphere.

only been possible for the eruptions with the largest signals: Kasatochi (August 2008), Redoubt (March 2009), Sarychev (June 2009), Merapi (November 2010), Puyehue-Cordón Caulle (June 2011) and Nabro (June 2011). This is indicated as extrapolation method "c" in Table 3. For the other eruptions typical lifetimes have been assumed as the average lifetimes of Kasatochi, Sarychev and Nabro ($\bar{\tau}_{\Delta h_1} = 13.3$ days, $\bar{\tau}_{\Delta h_2} = 23.6$ days, $\bar{\tau}_{\Delta h_3} = 32.3$ days). Thus, in those cases only the SO₂ masses $M_{\Delta h_i}(t_0)$ have been fitted. In Table 3 this is marked as extrapolation methods "a" or "b" where "a" means that only one enhanced value of $M_{\Delta h_i}(t)$ has been

used after the eruption while "b" indicates that more than one value of $M_{\Delta h_i}(t)$ has been fitted.

Uncertainties, which are given in brackets in Table 3, have been estimated by variation of the fitting interval time in case of methods "b" and "c". Additionally, for the cases "a" and "b" where lifetimes have not been derived simultaneously, an error of 20 % in the assumed values of $\bar{\tau}_{\Delta h_i}$ has been applied. The table also presents results of SO₂ mass and lifetime from previous studies. These are mainly based on nadir sounding satellite observations with the exception of Pumphrey et al. (2015), who discuss Aura/MLS limb measurements.

Table 3. Volcanic eruptions observed in MIPAS measurements. General data of volcanoes are obtained from http://www.volcano.si.edu. "TropVolc" indicate unidentified sources at low tropical latitudes. $M(t_0)$ are the resulting emission masses of SO$_2$ from the exponential fit (see text for details). Values of $M(t_0)$ are given for altitude ranges 10–14/14–18/18–22/**10–22** km. "$\tau =$" in column $M(t_0)$ indicates that a fit of the lifetime was possible with the values in days given for the altitude ranges 10–14/14–18/18–22 km. Values in brackets indicate estimated errors.

	Name	Eruption date	Location °N/°E	$M(t_0)$ [Gg] if present: τ [d]	$M(t_0)$ [Gg] if present: τ [d] from other sources
Ny	Nyamuragira	25 Jul 2002	−1.4/29.2	22(1)/12(1)/3(0)/**37(2)**[a]	
Ru	Ruang	25 Sep 2002	2.3/125.4	36(19)/39(9)/15(2)/**90(21)**[b]	74[1]
Rev	Reventador	03 Nov 2002	−0.1/−77.7	54(47)/29(6)/12(2)/**94(47)**[b]	65–84[1]; 100[2]
So	Soufrière Hills	12 Jul 2003	16.7/−62.2	68(19)/28(7)/2(1)/**98(20)**[b]	100–128[3]; 140[1]
Ma	Manam	27 Jan 2005	−4.1/145.0	79(15)/87(9)/39(3)/**206(17)**[a]	180[1]; 99 ± 13(> 68.1 hPa)[4]
An	Anatahan	06 Apr 2005	16.4/145.7	34(11)/34(7)/0(0)/**68(13)**[a]	165[1]
Tr	TropVolc	mid-Jul 2005	0.0/0.0	38(17)/21(5)/1(0)/**60(18)**[a]	
Tr	TropVolc	mid-Aug 2005	0.0/0.0	61(26)/23(5)/3(1)/**88(27)**[a]	
Ma	Manam	27 Feb 2006	−4.1/145.0	21(4)/58(8)/1(0)/**80(9)**[a]	
So	Soufrière Hills	20 May 2006	16.7/−62.2	40(29)/38(4)/85(15)/**162(33)**[a]	200[1]; 123–233[5]; 139 ± 24(> 68.1 hPa)[4]
Ra	Rabaul	7 Oct 2006	−4.3/152.2	75(26)/118(34)/12(4)/**205(43)**[b]	125[1]; 230[2]; 190 ± 14(> 100 hPa)[4]
Ny	Nyamuragira	27 Nov 2006	−1.4/29.2	49(6)/5(0)/–/**54(6)**[a]	58–216[1]
Fo	Fournaise, Piton de la	04 Apr 2007	−21.2/55.7	57(10)/12(1)/2(1)/**71(10)**[a]	140(> 7.5 km)[6]
Ta	Tair, Jebel at	30 Sep 2007	15.6/41.8	26(11)/27(5)/3(1)/**56(12)**[b]	46–57[7]
Ch	Chaiten	02 May 2008	−42.8/−72.7	26(7)/2(0)/2(0)/**30(7)**[a]	10[8]; 6[9]
Ok	Okmok	12 Jul 2008	53.4/−168.1	110(41)/31(6)/2(0)/**143(41)**[b]	200–300[5]; 100–200[10]
Ka	Kasatochi	07 Aug 2008	52.2/−175.5	645(127)/210(86)/43(8)/**899(154)**[c]	900–2700[11]; 2200[12]; 1000(> 10 km)[13] 1200[5]; 1700[9]; 1600[14]; 1350 ± 38(> 215 hPa)[4]
				$\tau = 14(1)/23(5)/32(4)$	$\tau = 8$–9[12]; 18[9]; ≈10[14]; 27 ± 1(> 215 hPa)[4]
Da	Dalaffilla	03 Nov 2008	13.8/40.5	31(9)/47(10)/1(0)/**79(13)**[b]	100–200[15]
Re	Redoubt	23 Mar 2009	60.5/−152.7	182(10)/18(7)/–/**200(12)**[c]	225–335[16]
				$\tau = 24(1)/22(6)/–$	
Fe	Fernandina	10 Apr 2009	−0.4/−91.6	14(2)/11(3)/2(0)/**27(4)**[a]	
Sa	Sarychev	12 Jun 2009	48.1/153.2	888(293)/542(60)/44(4)/**1473(299)**[c]	1200[17]; 900[14]; 571 ± 42(> 147 hPa)[4] 1160 ± 180(> 215 hPa)[4]
				$\tau = 15(2)/25(1)/38(2)$	$\tau = 27 ± 2(> 147$ hPa)[4]; 17 ± 3(> 215 hPa)[4]; $\tau = 10$–11[17]; ≈10[14]
Ny	Nyamuragira	02 Jan 2010	−1.4/29.2	17(5)/3(1)/2(0)/**22(6)**[b]	
So	Soufrière Hills	11 Feb 2010	16.7/−62.2	11(3)/12(2)/5(1)/**28(4)**[b]	50[18]
Pa	Pacaya	28 May 2010	14.4/−90.6	–/10(2)/4(1)/**14(2)**[b]	20[19]
Me	Merapi	04 Nov 2010	−7.5/110.4	–/253(61)/23(7)/**276(61)**[c]	440[20]
				$\tau = –/15(2)/24(7)$	
Sh	Shiveluch	12 Dec 2010	56.7/161.4	18(4)/1(0)/0(0)/**20(4)**[a]	
Kar	Karymsky	01 Jan 2011	54.0/159.4	–/–/1(0)/**1(0)**[a]	
Gr	Grímsvötn	21 May 2011	64.4/−17.3	273(101)/2(0)/–/**276(101)**[a]	350–400[14]; 108 ± 11(> 215 hPa)[4]
Pu	Puyehue-Cordón Caulle	04 Jun 2011	−40.6/−72.1	185(33)/–/–/**185(33)**[c]	250[14]
				$\tau = 32(3)/–/–$	$\tau = 6.8$[22]
Na	Nabro	12 Jun 2011	13.4/41.7	131(86)/343(79)/65(5)/**539(117)**[c]	1500[14]; 650(> 10 km)[21] 543 ± 45(> 147 hPa)[4]
				$\tau = 11(3)/23(2)/ 27(1)$	$\tau = 20 ± 2(> 147$ hPa)[4]

[a], [b], [c] extrapolation method, see Sect. 3.2. [1] Prata and Bernardo (2007), [2] Carn et al. (2009), [3] Carn and Prata (2010), [4] Pumphrey et al. (2015), [5] Prata et al. (2010), [6] Tulet and Villeneuve (2011), [7] Clarisse et al. (2008), [8] Neely et al. (2013, Table S1) and references therein, [9] Karagulian et al. (2010), [10] Spinei et al. (2010), [11] Corradini et al. (2010), [12] Krotkov et al. (2010), [13] Kristiansen et al. (2010), [14] Clarisse et al. (2012), [15] http://www.volcano.si.edu/volcano.cfm?vn=221070; S. Carn, personal communication, 2014, [16] Lopez et al. (2013), [17] Haywood et al. (2010), [18] Cole et al. (2010), [19] derived from Aura/OMI–30 May 2010 (http://so2.gsfc.nasa.gov), [20] Surono et al. (2012), [21] Clarisse et al. (2014), [22] Theys et al. (2013).

For an easier overview, a graphical representation of MIPAS total masses in comparison with external work is given in Fig. 15 where black symbols indicate MIPAS, red ones MLS and other colours the nadir observations. From a total of 42 pairs of MIPAS/external observations, 18 compare well within 1σ and 28 within 2σ error bars. Furthermore, about two-thirds (28 of 42) of the MIPAS-derived SO$_2$ masses are lower than those derived from other sources. This might be explained by the fact that nadir instruments sample the whole column of SO$_2$ while the MIPAS altitude range considered
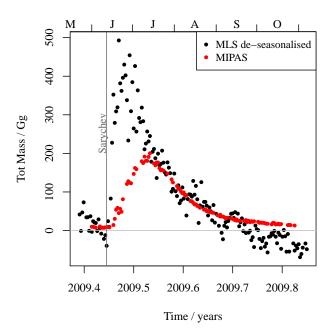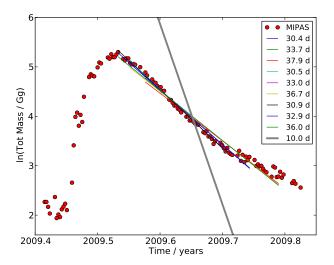
Figure 13. Comparison between daily values of global mass of SO$_2$ above 146.8 hPa after the Sarychev eruption from MIPAS (red) and from MLS deseasonalized observations (black) (Pumphrey et al., 2015).

Figure 14. Logarithmic representation of total mass of SO$_2$ above 146.8 hPa from MIPAS (red dots) from Fig. 13 in comparison with e-folding lifetime τ (thin solid lines) resulting from exponential fits using different start/end dates of the fit window. The bold grey line shows a fit with a fixed lifetime of 10 days.

here starts at 10 km, which leads to low MIPAS columns in cases where the bulk of SO$_2$ remains in the troposphere. Regarding only limb sounders, MIPAS total masses compare within the uncertainties with MLS for So06, Ra06, Sa09 (retrieval above 215 hPa) and Na11 while MIPAS values are lower for Ka08 and higher for Ma05 and Gr11. However, under consideration of the lower pressure level given for the MLS data set, MIPAS data of Ma05, So06 and Ra06 would be outside the estimated error range and lower than MLS.

For some of the volcanic eruptions detected in the MIPAS data set (see Table 3), no published values of emitted SO$_2$ abundances have been found. We attributed those SO$_2$ plumes to specific volcanic eruptions by comparison with measurements from nadir sounding satellites given at http://so2.gsfc.nasa.gov or at http://sacs.aeronomie.be. Furthermore, in two cases (mid-July and mid-August 2005) enhanced values of SO$_2$ have been detected, but due to the sparse data coverage by MIPAS during this time it was not possible to directly attribute those to specific eruptions.

Regarding the retrieved atmospheric e-folding lifetimes of SO$_2$, we could detect a clear dependence on altitude. Considering the major eruptions of Kasatochi in 2008 (Ka08), Sarychev in 2009 (Sa09) and Nabro in 2011 (Na11), these vary from 11–15 days at 10–14 km via 23–25 days at 14–18 km to 27–38 days at 18–22 km. These values are similar to those of MLS (Pumphrey et al., 2015), which derived 17 days above 215 hPa (11–12 km) and 27 days above 147 hPa (13–14 km) in the case of Sa09. From nadir sounders in the case of Ka08, Karagulian et al. (2010) derived a life-
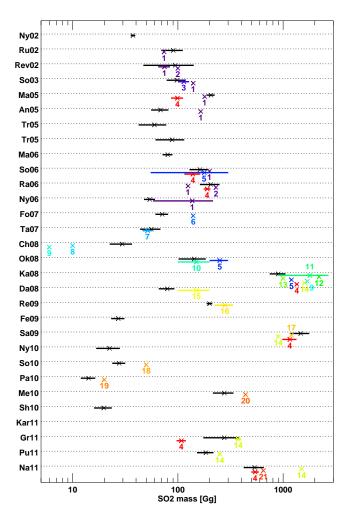
time of 18 days. This value, however, has been challenged by Clarisse et al. (2012), who determined similar values as reported by Krotkov et al. (2010): 8–9 days. For Sa09, Clarisse et al. (2012) showed a time dependence comparable to Haywood et al. (2010), pointing to a lifetime of around 10 days. Thus, there is a clear difference between SO$_2$ lifetime estimates from nadir and from limb-sounding instruments. Figure 14 illustrates this discrepancy by comparing a decay time of 10 days to the MIPAS observations from Fig. 13 in logarithmic representation. Haywood et al. (2010) have noted a similar difference between their nadir sounding observations and results from model runs. These differences have partly been explained by the SO$_2$ detection limit of the nadir measurements leading to lower lifetime estimates upon dispersion of the plume. A further contribution might also stem from the vertical sensitivity of nadir sounding instruments in combination with vertically varying decay times of SO$_2$: nadir sounders also sample air from altitudes lower in the troposphere which are not seen by the limb instruments and where the lifetime of SO$_2$ is probably shorter than at higher altitudes.

3.3 Global variability of background SO$_2$

A modulation of the SO$_2$ time series which seems not to be caused by volcanic activity appears in the Northern Hemisphere at mid- and high latitudes (see the top row in Fig. 10): in summer the SO$_2$ volume mixing ratios at 10 km altitude are enhanced with monthly mean values reaching 80–100 pptv. This feature can best be detected during years when volcanic influence was comparably small, such as 2003, 2007 or 2010. In comparison, northern wintertime volume mixing

Figure 15. Graphical representation of total SO$_2$ eruption masses as listed in Table 3. Black: MIPAS, red: MLS, other colours: nadir instruments. The coloured numbers refer to the references given in Table 3.
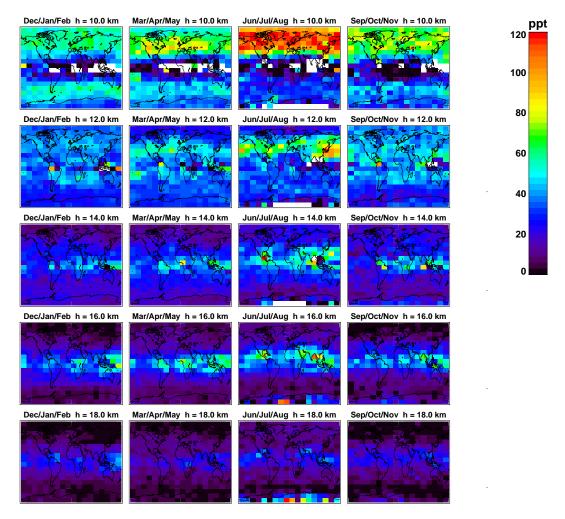
latitudes as already mentioned above. Furthermore, at 12 km one can observe the highest values of SO$_2$ over the western Pacific and Atlantic at northern subtropical and mid-latitudes in June–July–August (JJA). Enhanced values spread within this latitude band eastward over the Pacific and the Atlantic. Higher up, at 14 and 16 km, localized regions with enhanced SO$_2$ mixing ratios can be found over South East Asia, the Arabian Peninsula and middle America. At 18 km these locations of slightly enhanced values are still visible in JJA. Furthermore, at this altitude there appear enhanced mixing ratios over the Antarctic region which are probably connected to the downwelling of SO$_2$-rich air within the Antarctic polar vortex as described by Höpfner et al. (2013).

Comparison of these global structures and temporal variations in the UTLS with previous in situ measurements is difficult due to their sparsity and the variability of the observed SO$_2$ concentrations. The main feature of the MIPAS data set at lowest altitudes of 10 km, the annual variation with maximum values in JJA, cannot clearly be identified in available airborne in situ measurements (cf. Figs. 7 and 8). In situ campaigns providing data in northern mid-latitudes during summer have been e.g. ACCESS, ITOP, TACTS and DC3 (Fig. 8). During ACCESS and TACTS mean volume mixing ratios on the order of 30 pptv have been detected at around 10 km altitude while the corresponding MIPAS data show about 50–70 pptv. During ITOP and DC3, however, the MI-PAS values are more similar to the airborne averaged data of around 40–70 pptv. Thus, at the present stage, we cannot decide whether the annual variation of SO$_2$ at 10 km altitude is robust or caused by unknown artifacts within the MIPAS retrieval.

A similar interhemispheric picture of the SO$_2$ distribution as in the MIPAS data set has been obtained by Thornton et al. (1999) during flights over the Pacific. At 8–12 km altitude a north–south gradient has been found with values of 50–150 pptv in the north decreasing to 10 pptv at southern remote areas. (The Thornton et al. (1999) data are also included in the comparison of Fig. 7.)

Another feature reported by Thornton et al. (1999) and present also in the MIPAS distributions, especially in JJA (cf. Fig. 16), is the signal of pollution visible in the western North Pacific region east of the Asian continent and reaching even the upper troposphere. Enhanced levels of SO$_2$ in the free troposphere originating from the North China Plain have been observed by Ding et al. (2009) during airborne measurements in summer 2007. By trajectory analysis Ding et al. (2009) concluded that these polluted air masses are further lifted into the upper troposphere by warm conveyor belts. Furthermore, Fiedler et al. (2009a, b) report on measurements of enhanced SO$_2$ concentrations over Europe with origin in East Asia.

Enhanced concentrations of SO$_2$ at around 16–18 km located mainly in the regions of the Asian and the North American monsoons cannot be compared to in situ data due to the lack of observations at those altitudes. However, there may be a connection with the Asian tropopause aerosol

ratios of SO$_2$ are around 40–50 pptv. An annual cycle of SO$_2$ is also slightly visible at mid-latitudes in the Southern Hemisphere, however, with strongly reduced amplitude compared to the north (10 pptv in winter vs. 40 pptv in summer).

A globally resolved view on the seasonal variability of the SO$_2$ non-volcanic "background" is provided in Fig. 16. Here we have tried to exclude periods of direct volcanic SO$_2$ influence by visual inspection of single observations (as in Fig. 9) and of the overview plots (Figs. 10–12). Time periods which have been excluded from the analysis are reported in the caption of Fig. 16. Certainly it is not possible to exclude all volcanic influence. However, we tried to avoid the signals of the larger volcanic eruptions in order to get a picture of possible non-volcanic impact, its global distribution and its temporal modulation.

The most obvious temporal variability in background SO$_2$ is an annual cycle at 10 km altitude with maxima during summer over northern mid- to high latitudes and southern mid-

Figure 16. Seasonal global SO₂ background distributions at different altitude levels based on all MIPAS observations. The following time periods have been left out to avoid volcanic contributions: October–December 2002, July–August 2003, January–August 2005, May–November 2006, October–November 2007, July 2008–January 2009, April–December 2009, November–December 2010, June–October 2011.

layer (ATAL) which was detected in data of the space-borne lidar CALIPSO (Vernier et al., 2011a). There is a region of enhanced aerosol backscatter signal in the region of the Asian monsoon extending vertically from around 13 to 18 km. A similar but less pronounced aerosol feature is also present in connection with the North American monsoon (Vernier et al., 2011a). The nature of these particles is still unclear. Due to their low depolarization signal, either spherical droplets or small solid particles are candidates (Vernier et al., 2011a). The present MIPAS data indicate that there are enhanced levels of SO₂ in the monsoon regions at the altitudes of the ATAL. This points towards the possibility of a production of sulfate aerosols from SO₂ oxidation at those levels.

4 Conclusions

We have presented a data set of global SO₂ volume mixing ratio distributions which is complementary to the one shown in Höpfner et al. (2013). While the latter covers the altitude range of 15–40 km, the present retrievals extend from the upper troposphere up to about 20 km. In terms of temporal and horizontal resolution, the Höpfner et al. (2013) data are monthly and zonal average values of 10° latitudinal bins, while the new data record consists of single limb-scan retrievals from MIPAS/Envisat comprising more than 1000 profiles with global coverage daily. The estimated total error for single vmr profiles is typically in the range of 60–100 pptv. The error budget is dominated by the measurement noise. Other error contributions are estimated from about 10 pptv up to 100 pptv, with increasing errors towards lower altitudes. Comparison of the MIPAS SO₂ measurements with those of the ACE-FTS instrument revealed an

altitude-dependent offset in the background SO$_2$ concentrations of the second major measurement period of MIPAS (2005–2012). The two periods have been debiased by the application of a height- and latitude-dependent correction field yielding residual biases of less than 20 pptv. Due to the sparsity of in situ observations of SO$_2$, no systematic validation could be made with collocated measurements. However, we could compare within similar latitudes and seasons of the year. This resulted in a scatter of the differences within about ±50 pptv, revealing no indication for a problem with the actual MIPAS data after debiasing.

Due to the global coverage of this data set and the high sensitivity of limb observations, the evolution of SO$_2$ clouds from single volcanic eruptions reaching the region of the UTLS can be tracked, in some cases for even more than half a year. We have derived volcanic injection masses and for some cases also atmospheric lifetimes at three altitude regions for 30 eruptions between 2002 and 2012. The determination of masses of emitted SO$_2$ was complicated due to an underestimation of the total mass directly after the eruptions which has become evident by a comparison with SO$_2$ masses derived from MLS. This is attributed to sampling artifacts caused by the discard of MIPAS spectra with large aerosol contribution, an effect similar to the "aerosol cloud top" feature in SAGE II observations (McCormick and Veiga, 1992; Fromm et al., 2014) and the smearing of SO$_2$ profile maxima in case of extremely high mixing ratios where the spectral lines are saturated and, thus, carry less information. The derived masses can be used as input for atmospheric models taking into account explicitly also smaller volcanic eruptions reaching stratospheric levels. Furthermore, to our knowledge for the first time the atmospheric e-folding lifetime of SO$_2$ has been derived at different levels in the UTLS. The average lifetimes increase with altitude from about 13 days at 10–14 km up to 32 days at 18–22 km. These values are compatible with other limb-sounding measurements (Pumphrey et al., 2015) but are considerably larger than estimates from nadir sounders. We attribute this discrepancy to the SO$_2$ detection limit of nadir sounding instruments and a combination of both decay time and instrument sensitivity varying with height.

Seasonal global maps of background SO$_2$ distributions are provided by omitting volcanically perturbed periods. In the northern mid- and high latitudes at about 10 km altitude these maps indicate an annual cycle with maximum values during summertime. Candidate explanations are the higher tropopause level during summer and the so-called flushing of the extratropical UTLS with tropospheric air from late spring to summer (Gettelman et al., 2011, and references therein). To our knowledge, such a cycle in SO$_2$ has not been observed before. However, the significance of this particular result is limited, and additional measurements are needed for confirmation or falsification. The same applies to increased concentrations of SO$_2$ at altitudes of 16–18 km at the regions and during the period of the Asian and North American monsoon,

which might be linked to the ATAL (Vernier et al., 2011a). This calls for a closer probing of upper altitude monsoon airmasses with respect to sulfur species which is actually a goal of the StratoClim project (http://www.stratoclim.org/).

The Supplement related to this article is available online at doi:10.5194/acp-15-7017-2015-supplement.

References

Barth, M. C., Cantrell, C. A., Brune, W. H., Rutledge, S. A., Crawford, J. H., Huntrieser, H., Carey, L. D., MacGorman, D., Weisman, M., Pickering, K. E., Bruning, E., Anderson, B., Apel, E., Biggerstaff, M., Campos, T., Campuzano-Jost, P., Cohen, R., Crounse, J., Day, D. A., Diskin, G., Flocke, F., Fried, A., Garland, C., Heikes, B., Honomichl, S., Hornbrook, R., Huey, L. G., Jimenez, J. L., Lang, T., Lichtenstern, M., Mikoviny, T., Nault, B., O'Sullivan, D., Pan, L. L., Peischl, J., Pollack, I., Richter, D., Riemer, D., Ryerson, T., Schlager, H., Clair, J. S., Walega, J., Weibring, P., Weinheimer, A., Wennberg, P., Wisthaler, A., Wooldridge, P. J., and Ziegler, C.: The Deep Convective Clouds and Chemistry (DC3) Field Campaign, B. Am. Meteorol. Soc., doi:10.1175/BAMS-D-13-00290.1, 2014.

Bernath, P. F., McElroy, C. T., Abrams, M. C., Boone, C. D., Butler, M., Camy-Peyret, C., Carleer, M., Clerbaux, C., Coheur, P.-F., Colin, R., DeCola, P., DeMazière, M., Drummond, J. R., Dufour, D., Evans, W. F. J., Fast, H., Fussen, D., Gilbert, K., Jennings, D. E., Llewellyn, E. J., Lowe, R. P., Mahieu, E., McConnell, J. C., McHugh, M., McLeod, S. D., Michaud, R., Midwinter, C., Nassar, R., Nichitiu, F., Nowlan, C., Rinsland, C. P., Rochon, Y. J., Rowlands, N., Semeniuk, K., Simon, P., Skelton, R., Sloan, J. J., Soucy, M.-A., Strong, K., Tremblay, P., Turnbull, D., Walker, K. A., Walkty, I., Wardle, D. A., Wehrle, V., Zander, R., and Zou, J.: Atmospheric Chemistry Experiment

(ACE): Mission overview, Geophys. Res. Lett., 32, L15S01, doi:10.1029/2005GL022386, 2005.

Carboni, E., Grainger, R., Walker, J., Dudhia, A., and Siddans, R.: A new scheme for sulphur dioxide retrieval from IASI measurements: application to the Eyjafjallajökull eruption of April and May 2010, Atmos. Chem. Phys., 12, 11417–11434, doi:10.5194/acp-12-11417-2012, 2012.

Carn, S. A. and Prata, F. J.: Satellite-based constraints on explosive SO₂ release from Soufrière Hills Volcano, Montserrat, Geophys. Res. Lett., 37, L00E22, doi:10.1029/2010GL044971, 2010.

Carn, S. A., Krueger, A. J., Krotkov, N. A., Yang, K., and Evans, K.: Tracking volcanic sulfur dioxide clouds for aviation hazard mitigation, Nat. Hazards, 51, 325–343, doi:10.1007/s11069-008-9228-4, 2009.

Clarisse, L., Coheur, P. F., Prata, A. J., Hurtmans, D., Razavi, A., Phulpin, T., Hadji-Lazaro, J., and Clerbaux, C.: Tracking and quantifying volcanic SO₂ with IASI, the September 2007 eruption at Jebel at Tair, Atmos. Chem. Phys., 8, 7723–7734, doi:10.5194/acp-8-7723-2008, 2008.

Clarisse, L., Hurtmans, D., Clerbaux, C., Hadji-Lazaro, J., Ngadi, Y., and Coheur, P.-F.: Retrieval of sulphur dioxide from the infrared atmospheric sounding interferometer (IASI), Atmos. Meas. Tech., 5, 581–594, doi:10.5194/amt-5-581-2012, 2012.

Clarisse, L., Coheur, P.-F., Theys, N., Hurtmans, D., and Clerbaux, C.: The 2011 Nabro eruption, a SO₂ plume height analysis using IASI measurements, Atmos. Chem. Phys., 14, 3095–3111, doi:10.5194/acp-14-3095-2014, 2014.

Cole, P., Bass, V., Christopher, C., Fergus, M., Gunn, L., Odbert, H., Simpson, R., Stewart, R., Stinton, A., Stone, J., Syers, R., Robertson, R., Watts, R., and Williams, P.: Report to the Scientific Advisory Committee on Montserrat Volcanic Activity, Report on Activity between 15 August 2009 and 28 February 2010, Tech. rep., Montserrat Volcano Observatory, open File Report OFR 10-01a, Montserrat, 2010.

Corradini, S., Merucci, L., Prata, A. J., and Piscini, A.: Volcanic ash and SO₂ in the 2008 Kasatochi eruption: retrievals comparison from different IR satellite sensors, J. Geophys. Res., 115, D00L21, doi:10.1029/2009JD013634, 2010.

Curtius, J., Sierau, B., Arnold, F., de Reus, M., Ström, J., Scheeren, H. A., and Lelieveld, J.: Measurement of aerosol sulfuric acid: 2. Pronounced layering in the free troposphere during the second Aerosol Characterization Experiment (ACE 2), J. Geophys. Res., 106, 31975, doi:10.1029/2001JD000605, 2001.

Ding, A., Wang, T., Xue, L., Gao, J., Stohl, A., Lei, H., Jin, D., Ren, Y., Wang, X., Wei, X., Qi, Y., Liu, J., and Zhang, X.: Transport of north China air pollution by midlatitude cyclones: case study of aircraft measurements in summer 2007, J. Geophys. Res., 114, D08304, doi:10.1029/2008JD011023, 2009.

Doeringer, D., Eldering, A., Boone, C. D., González Abad, G., and Bernath, P. F.: Observation of sulfate aerosols and SO₂ from the Sarychev volcanic eruption using data from the Atmospheric Chemistry Experiment (ACE), J. Geophys. Res., 117, D03203, doi:10.1029/2011JD016556, 2012.

ESA: Envisat MIPAS: An instrument for atmospheric chemistry and climate research, Tech. Rep. SP-1229, European Space Agency, SA Publications Division, ESTEC, P. O. Box 299, 2200 AG Noordwijk, the Netherlands, 2000.

Fiedler, V., Arnold, F., Schlager, H., Dörnbrack, A., Pirjola, L., and Stohl, A.: East Asian SO₂ pollution plume over Europe – Part 2:

Evolution and potential impact, Atmos. Chem. Phys., 9, 4729–4745, doi:10.5194/acp-9-4729-2009, 2009a.

Fiedler, V., Nau, R., Ludmann, S., Arnold, F., Schlager, H., and Stohl, A.: East Asian SO₂ pollution plume over Europe – Part 1: Airborne trace gas measurements and source identification by particle dispersion model simulations, Atmos. Chem. Phys., 9, 4717–4728, doi:10.5194/acp-9-4717-2009, 2009b.

Fiedler, V., Arnold, F., Ludmann, S., Minikin, A., Hamburger, T., Pirjola, L., Dörnbrack, A., and Schlager, H.: African biomass burning plumes over the Atlantic: aircraft based measurements and implications for H₂SO₄ and HNO₃ mediated smoke particle activation, Atmos. Chem. Phys., 11, 3211–3225, doi:10.5194/acp-11-3211-2011, 2011.

Fischer, H., Birk, M., Blom, C., Carli, B., Carlotti, M., von Clarmann, T., Delbouille, L., Dudhia, A., Ehhalt, D., Endemann, M., Flaud, J. M., Gessner, R., Kleinert, A., Koopman, R., Langen, J., López-Puertas, M., Mosner, P., Nett, H., Oelhaf, H., Perron, G., Remedios, J., Ridolfi, M., Stiller, G., and Zander, R.: MIPAS: an instrument for atmospheric and climate research, Atmos. Chem. Phys., 8, 2151–2188, doi:10.5194/acp-8-2151-2008, 2008.

Fromm, M., Kablick, G., Nedoluha, G., Carboni, E., Grainger, R., Campbell, J., and Lewis, J.: Correcting the record of volcanic stratospheric aerosol impact: Nabro and Sarychev peak, J. Geophys. Res., 119, 10343–10364, doi:10.1002/2014JD021507, 2014.

Fyfe, J. C., Gillett, N. P., and Zwiers, F. W.: Overestimated global warming over the past 20 years, Nature Clim. Change, 3, 767–769, doi:10.1038/nclimate1972, 2013a.

Fyfe, J. C., von Salzen, K., Cole, J. N. S., Gillett, N. P., and Vernier, J.-P.: Surface response to stratospheric aerosol changes in a coupled atmosphere–ocean model, Geophys. Res. Lett., 40, 584–588, doi:10.1002/grl.50156, 2013b.

Gettelman, A., Hoor, P., Pan, L. L., Randel, W. J., Hegglin, M. I., and Birner, T.: The extratropical upper troposphere and lower stratoshpere, Rev. Geophys., 49, RG3003, doi:10.1029/2011RG000355, 2011.

Haywood, J. M., Jones, A., Clarisse, L., Bourassa, A., Barnes, J., Telford, P., Bellouin, N., Boucher, O., Agnew, P., Clerbaux, C., Coheur, P., Degenstein, D., and Braesicke, P.: Observations of the eruption of the Sarychev volcano and simulations using the HadGEM2 climate model, J. Geophys. Res., 115, D21212, doi:10.1029/2010JD014447, 2010.

Haywood, J. M., Jones, A., and Jones, G. S.: The impact of volcanic eruptions in the period 2000–2013 on global mean temperature trends evaluated in the HadGEM2-ES climate model, Atmos. Sci. Lett., 15, 92–96, doi:10.1002/asl2.471, 2013.

Hofmann, D., Barnes, J., O'Neill, M., Trudeau, M., and Neely, R.: Increase in background stratospheric aerosol observed with lidar at Mauna Loa Observatory and Boulder, Colorado, Geophys. Res. Lett., 36, L15808, doi:10.1029/2009GL039008, 2009.

Höpfner, M., Glatthor, N., Grabowski, U., Kellmann, S., Kiefer, M., Linden, A., Orphal, J., Stiller, G., von Clarmann, T., Funke, B., and Boone, C. D.: Sulfur dioxide (SO₂) as observed by MIPAS/Envisat: temporal development and spatial distribution at 15–45 km altitude, Atmos. Chem. Phys., 13, 10405–10423, doi:10.5194/acp-13-10405-2013, 2013.

Inn, E. C. Y. and Vedder, J. F.: Measurements of stratospheric sulfur constituents, Geophys. Res. Lett., 8, 5–8, 1981.

Jaeschke, W., Georgii, H.-W., and Schmitt, R.: Preliminary results of stratospheric SO$_2$ measurements, Geophys. Res. Lett., 3, 517–519, 1976.

Jaeschke, W., Salkowski, T., Dierssen, J., Trümbach, J., Krischke, U., and Günther, A.: Measurements of trace substances in the Arctic Troposphere as potential precursors and constituents of arctic haze, J. Atmos. Chem., 34, 291–319, doi:10.1023/A:1006277230042, 1999.

Karagulian, F., Clarisse, L., Clerbaux, C., Prata, A. J., Hurtmans, D., and Coheur, P. F.: Detection of volcanic SO$_2$, ash, and H$_2$SO$_4$ using the Infrared Atmospheric Sounding Interferometer (IASI), J. Geophys. Res., 115, D00L02, doi:10.1029/2009JD012786, 2010.

Kristiansen, N. I., Stohl, A., Prata, A. J., Richter, A., Eckhardt, S., Seibert, P., Hoffmann, A., Ritter, C., Bitar, L., Duck, T. J., and Stebel, K.: Remote sensing and inverse transport modeling of the Kasatochi eruption sulfur dioxide cloud, J. Geophys. Res., 115, D00L16, doi:10.1029/2009JD013286, 2010.

Krotkov, N. A., Schoeberl, M. R., Morris, G. A., Carn, S., and Yang, K.: Dispersion and lifetime of the SO$_2$ cloud from the August 2008 Kasatochi eruption, J. Geophys. Res., 115, D00L20, doi:10.1029/2010JD013984, 2010.

Lopez, T., Carn, S., Werner, C., Fee, D., Kelly, P., Doukas, M., Pfeffer, M., Webley, P., Cahill, C., and Schneider, D.: Evaluation of Redoubt Volcano's sulfur dioxide emissions by the Ozone Monitoring Instrument, J. Volcanol. Geoth. Res., 259, 290–307, doi:10.1016/j.jvolgeores.2012.03.002, 2013.

McCormick, M. P. and Veiga, R. E.: SAGE II measurements of early Pinatubo aerosols, Geophys. Res. Lett., 19, 155–158, doi:10.1029/91GL02790, 1992.

Meixner, F. X.: The vertical sulfur dioxide distribution at the tropopause level, J. Atmos. Chem., 2, 175–189, 1984.

Möhler, O.,and Arnold, F.: Gaseous sulfuric acid and sulfur dioxide measurements in the Arctic troposphere and lower stratosphere: implications for hydroxyl radical abundances, Geophys. Res. Lett., 19, 1763–1766, 1992.

Neely, R. R., Toon, O. B., Solomon, S., Vernier, J. P., Alvarez, C., English, J. M., Rosenlof, K. H., Mills, M. J., Bardeen, C. G., Daniel, J. S., and Thayer, J. P.: Recent anthropogenic increases in SO$_2$ from Asia have minimal impact on stratospheric aerosol, Geophys. Res. Lett., 40, 999–1004, doi:10.1002/grl.50263, 2013.

Nett, H., Perron, G., Sanchez, M., Burgess, A., and Mossner, P.: MIPAS inflight calibration and processor validation, in: ENVISAT Calibration Review – Proc. of the European Workshop, 09–13 September 2002, ESTEC, Noordwijk, the Netherlands, edited by: Sawaya-Lacoste, H., vol. SP-520, ESA Publications Division, ESTEC, Postbus 299, 2200 AG Noordwijk, the Netherlands, 2002.

Prata, A. J. and Bernardo, C.: Retrieval of volcanic SO$_2$ column abundance from Atmospheric Infrared Sounder data, J. Geophys. Res., 112, D20204, doi:10.1029/2006JD007955, 2007.

Prata, A. J., Gangale, G., Clarisse, L., and Karagulian, F.: Ash and sulfur dioxide in the 2008 eruptions of Okmok and Kasatochi: insights from high spectral resolution satellite measurements, J. Geophys. Res., 115, D00L18, doi:10.1029/2009JD013556, 2010.

Pumphrey, H. C., Read, W. G., Livesey, N. J., and Yang, K.: Observations of volcanic SO$_2$ from MLS on Aura, Atmos. Meas. Tech., 8, 195–209, doi:10.5194/amt-8-195-2015, 2015.

Read, W. G., Froidevaux, L., and Waters, J. W.: Microwave limb sounder measurement of stratospheric SO$_2$ from the Mount Pinatubo volcano, Geophys. Res. Lett., 20, 1299–1302, doi:10.1029/93GL00831, 1993.

Reiner, T., Möhler, O., and Arnold, F.: Improved atmospheric trace gas measurements with an aircraft-based tandem mass spectrometer: ion identification by mass-selected fragmentation studies, J. Geophys. Res., 103, 31309, doi:10.1029/1998JD100003, 1998.

Ridley, D. A., Solomon, S., Barnes, J. E., Burlakov, V., Deshler, T., Dolgii, S., Herber, A., Nagai, T., Neely, R. R., Nevzorov, A., Ritter, C., Sakai, T., Santer, B. D., Sato, M., Schmidt, A., Uchino, O., and Vernier, J. P.: Total volcanic stratospheric aerosol optical depths and implications for global climate change, Geophys. Res. Lett., 41, 7763–7769, doi:10.1002/2014GL061541, 2014.

Rix, M., Valks, P., Hao, N., Loyola, D., Schlager, H., Huntrieser, H., Flemming, J., Koehler, U., Schumann, U., and Inness, A.: Volcanic SO$_2$, BrO and plume height estimations using GOME-2 satellite measurements during the eruption of Eyjafjallajökull in May 2010, J. Geophys. Res., 117, D00U19, doi:10.1029/2011JD016718, 2012.

Roiger, A., Thomas, J.-L., Schlager, H., Law, K. S., Kim, J., Schäfler, A., Weinzierl, B., Dahlkötter, F., Krisch, I., Marelle, L., Minikin, A., Raut, J.-C., Reiter, A., Rose, M., Scheibe, M., Stock, P., Baumann, R., Bouarar, I., Clerbaux, C., George, M., Onishi, T., and Flemming, J.: Quantifying emerging local anthropogenic emissions in the Arctic region: the ACCESS aircraft campaign experiment, B. Am. Meteorol. Soc., doi:10.1175/BAMS-D-13-00169.1, 2014.

Santer, B. D., Bonfils, C., Painter, J. F., Zelinka, M. D., Mears, C., Solomon, S., Schmidt, G. A., Fyfe, J. C., Cole, J. N. S., Nazarenko, L., Taylor, K. E., and Wentz, F. J.: Volcanic contribution to decadal changes in tropospheric temperature, Nat. Geosci., 7, 185–189, doi:10.1038/ngeo2098, 2014.

Schlager, H., Baumann, R., Lichtenstern, M., Petzold, A., Arnold, F., Speidel, M., Gurk, C., and Fischer, H.: Aircraft-based trace gas measurements in a primary European ship corridor, in: Proceedings of the TAC-Conference, 29 June 2006, Oxford, UK, 83–88, 2006.

Solomon, S., Daniel, J. S., Neely, R. R., Vernier, J.-P., Dutton, E. G., and Thomason, L. W.: The persistently variable "background" stratospheric aerosol layer and global climate change, Science, 333, 866–870, doi:10.1126/science.1206027, 2011.

Speidel, M., Nau, R., Arnold, F., Schlager, H., and Stohl, A.: Sulfur dioxide measurements in the lower, middle and upper troposphere: deployment of an aircraft-based chemical ionization mass spectrometer with permanent in-flight calibration, Atmos. Environ., 41, 2427–2437, doi:10.1016/j.atmosenv.2006.07.047, 2007.

Spinei, E., Carn, S. A., Krotkov, N. A., Mount, G. H., Yang, K., and Krueger, A.: Validation of ozone monitoring instrument SO$_2$ measurements in the Okmok volcanic cloud over Pullman, WA, July 2008, J. Geophys. Res., 115, D00L08, doi:10.1029/2009JD013492, 2010.

Steck, T.: Methods for determining regularization for atmospheric retrieval problems, Appl. Optics, 41, 1788–1797, 2002.

Surono, Jousset, P., Pallister, J., Boichu, M., Buongiorno, M. F., Budisantoso, A., Costa, F., Andreastuti, S., Prata, F., Schneider, D., Clarisse, L., Humaida, H., Sumarti, S., Bignami, C.,

Griswold, J., Carn, S., Oppenheimer, C., and Lavigne, F.: The 2010 explosive eruption of Java's Merapi volcano – A "100-year" event, J. Volcanol. Geoth. Res., 241, 121–135, doi:10.1016/j.jvolgeores.2012.06.018, 2012.

Theys, N., Campion, R., Clarisse, L., Brenot, H., van Gent, J., Dils, B., Corradini, S., Merucci, L., Coheur, P.-F., Van Roozendael, M., Hurtmans, D., Clerbaux, C., Tait, S., and Ferrucci, F.: Volcanic SO$_2$ fluxes derived from satellite data: a survey using OMI, GOME-2, IASI and MODIS, Atmos. Chem. Phys., 13, 5945–5968, doi:10.5194/acp-13-5945-2013, 2013.

Thornton, D. C., Bandy, A. R., Blomquist, B. W., Driedger, A. R., and Wade, T. P.: Sulfur dioxide distribution over the Pacific Ocean 1991–1996, J. Geophys. Res., 104, 5845–5854, 1999.

Tikhonov, A.: On the solution of incorrectly stated problems and method of regularization, Dokl. Akad. Nauk. SSSR, 151, 501–504, 1963.

Tulet, P. and Villeneuve, N.: Large scale modeling of the transport, chemical transformation and mass budget of the sulfur emitted during the April 2007 eruption of Piton de la Fournaise, Atmos. Chem. Phys., 11, 4533–4546, doi:10.5194/acp-11-4533-2011, 2011.

Van Gent, J., Spurr, R., Lerot, C., Van Roozendael, M., Theys, N., and Brenot, H.: SO$_2$ plume height retrieval from direct fitting of GOME-2 backscattered radiance measurements, in: 39th COSPAR Scientific Assembly, Held 14–22 July 2012, Mysore, India, Abstract C0.3-1-12, vol. 39 of COSPAR Meeting, 2012.

Vernier, J.-P., Thomason, L. W., and Kar, J.: CALIPSO detection of an Asian tropopause aerosol layer, Geophys. Res. Lett., 38, L07804, doi:10.1029/2010GL046614, 2011a.

Vernier, J.-P., Thomason, L. W., Pommereau, J.-P., Bourassa, A., Pelon, J., Garnier, A., Hauchecorne, A., Blanot, L., Trepte, C., Degenstein, D., and Vargas, F.: Major influence of tropical volcanic eruptions on the stratospheric aerosol layer during the last decade, Geophys. Res. Lett., 38, L12807, doi:10.1029/2011GL047563, 2011b.

von Clarmann, T., Glatthor, N., Grabowski, U., Höpfner, M., Kellmann, S., Kiefer, M., Linden, A., Mengistu Tsidu, G., Milz, M., Steck, T., Stiller, G. P., Wang, D. Y., Fischer, H., Funke, B., Gil-López, S., and López-Puertas, M.: Retrieval of temperature and tangent altitude pointing from limb emission spectra recorded from space by the Michelson Interferometer for Passive Atmospheric Sounding (MIPAS), J. Geophys. Res., 108, 4736, doi:10.1029/2003JD003602, 2003.

von Clarmann, T., Höpfner, M., Kellmann, S., Linden, A., Chauhan, S., Funke, B., Grabowski, U., Glatthor, N., Kiefer, M., Schieferdecker, T., Stiller, G. P., and Versick, S.: Retrieval of temperature, H$_2$O, O$_3$, HNO$_3$, CH$_4$, N$_2$O, ClONO$_2$ and ClO from MIPAS reduced resolution nominal mode limb emission measurements, Atmos. Meas. Tech., 2, 159–175, doi:10.5194/amt-2-159-2009, 2009.

Waddicor, D. A., Vaughan, G., Choularton, T. W., Bower, K. N., Coe, H., Gallagher, M., Williams, P. I., Flynn, M., Volz-Thomas, A., Pätz, H. -W., Isaac, P., Hacker, J., Arnold, F., Schlager, H., and Whiteway, J. A.: Aerosol observations and growth rates downwind of the anvil of a deep tropical thunderstorm, Atmos. Chem. Phys., 12, 6157–6172, doi:10.5194/acp-12-6157-2012, 2012.

Yang, K., Liu, X., Bhartia, P. K., Krotkov, N. A., Carn, S. A., Hughes, E. J., Krueger, A. J., Spurr, R. J. D., and Trahan, S. G.: Direct retrieval of sulfur dioxide amount and altitude from spaceborne hyperspectral UV measurements: Theory and application, J. Geophys. Res., 115, D00L09, doi:10.1029/2010JD013982, 2010.